J Mater Sci (2013) 48:4705–4712
DOI 10.1007/s10853-013-7151-x

NANOSTRUCTURED MATERIALS

Mechanical properties and microstructure evolution in ultrafine-grained AZ31 alloy processed by severe plastic deformation

Jitka Vrátná · Miloš Janeček · Jakub Čížek · Dong Jun Lee · Eun Yoo Yoon · Hyoung Seop Kim

Received: 10 November 2012 / Accepted: 9 January 2013 / Published online: 24 January 2013

Abstract Commercial MgAlZn alloy AZ31 was processed by two techniques of severe plastic deformation (SPD)—extrusion followed by equal channel angular pressing (EX-ECAP), and high pressure torsion (HPT). Processing by ECAP was conducted at elevated temperature of 180 °C for 1–12 passes following route B_C. HPT was applied at room temperature, and the specimens of the diameter of 19 mm with different number of turns ($N = ¼ - 15$) were prepared. Mechanical properties and grain fragmentation with strain due to EX-ECAP and HPT were investigated by Vickers microhardness measurements and transmission electron microscopy, respectively. Variations in dislocation density were investigated by positron annihilation spectroscopy. Differences in microhardness, grain refinement and dislocation density evolution resulting from principal differences of straining were found in the specimens. EX-ECAP resulted in homogeneous microstructure throughout the specimen's cross section as early as after four passes. On the other hand, laterally inhomogeneous microstructure with gradual reduction of grain sizes from the centre towards the periphery of the disk was observed in specimens after HPT. This microstructure and microhardness inhomogeneities were continuously smeared out and almost homogeneous ultrafine-grained structure was observed in specimen subjected to 15 HPT turns. Variations in mechanical properties and dislocation density evolution were compared in conditions corresponding to the same equivalent strain imposed by both techniques of SPD.

J. Vrátná · M. Janeček (✉)
Department of Physics of Materials, Faculty of Mathematics and Physics, Charles University, Prague, Czech Republic
e-mail: janecek@met.mff.cuni.cz

J. Čížek
Department of Low Temperature Physics, Faculty of Mathematics and Physics, Charles University, Prague, Czech Republic

D. J. Lee · E. Y. Yoon · H. S. Kim
Department of Materials Science and Engineering, POSTECH, Pohang 790-784, South Korea

Introduction

Magnesium alloys are energy-efficient materials with the potential to replace steel, aluminium alloys or some plastic-based materials in various applications. Interest in magnesium-based materials has recently been revived primarily because of gradually reducing costs of these materials and the resolve of scientists, researchers and engineers to cut down energy consumption and greenhouse gas emissions [1].

The mechanical and other essential properties determining the application of magnesium alloys may be improved by refining the grain size to submicrometre or even nanometre level. It is known that the structure of deformed metals can change with increasing plastic deformation so that the random dislocation arrays can lower the energy of the system by accumulation of dislocations into cells. The process results in high dislocation density in cell walls and low dislocation density within the cells. Subgrains, like cells, show small misorientations with their neighbours, but have sharper boundaries, and are formed by plastic deformation and thermal recovery processes [2]. A variety of special techniques are used for the production of bulk ultrafine-grained (UFG) materials, e.g. equal channel angular pressing (ECAP) [3], high-pressure torsion (HPT) [4, 5], accumulative roll-bonding (ARB) [6], twist extrusion [7] or multidirectional forging [8]. Among

these techniques, which introduce the severe plastic deformation (SPD) in the material, the HPT is a very efficient method of grain refinement [9]. HPT was also successfully applied for producing consolidated metal powders [10]. On the other hand, ECAP is quite an easy and widely used SPD technique.

Owing to an inhomogeneous strain introduced to the specimen by torsional straining (HPT) an inhomogeneous microstructural refinement occurs. As a consequence, the average grain size and mechanical properties differ across the cross section of the sample. It was shown that the strain inhomogeneity is reduced by increasing number of rotations [11]. After at least five or eight rotations (depending on material), almost homogeneous strain distribution was observed by several authors [11–13] who measured microhardness profiles through the specimen's cross section.

On the other hand, this apparent disadvantage of inhomogeneity is also eliminated when ring samples are used [14]. However, the small size of the samples is the main disadvantage of HPT method for applications in industry. Because of this limitation, material achieved by this technique is used mostly in modern micro-size specialized industrial branches. HPT has been successfully employed to several materials, e.g. pure nickel [11], aluminium [14], copper [15] magnesium [16], aluminium-CNT composites [17], copper-CNT composites [18], etc.

The objective of this article is to compare the mechanical properties, microstructure and dislocation structure evolution of the AZ31 magnesium alloy prepared by two different SPD methods–extrusion and equal channel angular pressing (EX-ECAP) and HPT.

Experimental procedures

Experimental material

Commercial AZ31 alloy with a nominal composition of Mg–3 %Al–1 %Zn in the initial as cast condition was used in this investigation. One set of the samples was prepared by extrusion and ECAP (EX-ECAP), the other one by HPT.

Prior to ECAP, the specimens were extruded at 350 °C with an extrusion ratio of 22. The ECAP die was equipped with an ejector that allows pushing the sample out of the die immediately after its pressing by a plunger from the feed-in channel to the exit channel. ECAP pressing was performed at 180 °C following route B_c, i.e. rotating the sample 90° between the individual passes, with the velocity of 50 mm/min and molybdenum disulphide grease was used as a lubricant. The angle Φ between two intersecting channels and the corner angle Ψ were 90° and 0°, respectively. Both channels have a square cross section of 10 × 10 mm.

Prior to HPT, the material was homogenized at 390 °C for 12 h. After homogenization, the disk specimens with the diameter of 19 mm and the thickness of 1–2 mm were cut from the billet. These specimens were processed by quasi-constrained HTP at room temperature for $N = ¼, ½, 1, 5$ and 15 rotations. The experimental setup is schematically illustrated in Fig. 1 [19]. In addition to samples subjected to various number N of HPT rotations, a sample which was pressed only between the anvils (STAGE I in Fig. 1) but not subjected to any HPT rotation ($N = 0$) was investigated as well.

The upper anvil is fixed with a load cell mounted on its top allowing measuring the hydrostatic pressure which is applied to the specimen during straining. The lower anvil with a sample placed in the groove is first lifted to its final position pressing the specimen to the symmetrical groove in the upper anvil. The upper and lower anvils of the die had depressions of 20-mm diameter and 0.25-mm thickness. The lateral wall was set at the angle of 5° to the vertical. In the compression stage, the speed of the top anvil was 0.1 mm/s until a pressure of 2.5 GPa was developed on the workpiece. In the torsion stage, the lower anvil was rotated at 0.1 rad/s up to a full turn with a constant pressure of 2.5 GPa. The friction between the die and the workpiece was set to satisfy the sticking condition, since the roughness of the die surface was high enough to prevent slippage between the workpiece and the die.

Positron annihilation spectroscopy measurements

A $^{22}Na_2CO_3$ positron source with the activity of 1.5 MBq was used in positron lifetime measurements. The source spot with diameter of 1 mm was deposited on a 2-μm-thick Mylar foil and sealed between two identical specimens of the studied material. The source contribution consists of two components with lifetimes of 368 ps (intensity 8 %) and 1.5 ns (intensity 1 %) which come from positrons annihilated in the $^{22}Na_2CO_3$ source spot and in the covering Mylar foil, respectively.

A fast–fast spectrometer [20] with the time resolution of 150 ps (FWHM ^{22}Na) was employed for positron lifetime measurements. At least, 10^7 positron annihilation events were accumulated in each positron lifetime spectrum which was subsequently decomposed into individual exponential components by a maximum likelihood procedure [21].

In order to examine homogeneity of UFG structure, positron lifetime measurements of HPT deformed samples were performed at various distances r from the centre of the sample disk corresponding to the rotation axis of torsion deformation. Measurements at various distances r were performed simply by moving the positron source spot from the centre of the sample towards its periphery and recording positron lifetime spectra at various distances

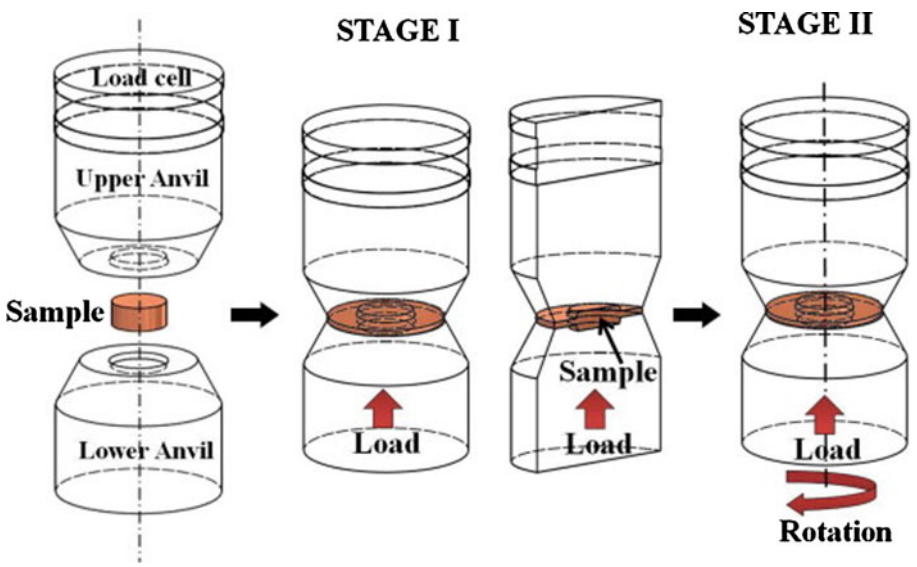

Fig. 1 Schematic illustration of the HPT device showing the set-up, compression stage (stage I) and compression–torsion stage (stage II) [19]

of the source spot from the centre. The uncertainty in position of the positron source was ~0.1 mm.

Microhardness measurements

Vickers microhardness HV0.1 was measured on a semi-automatic Wolpert tester allowing automatic indentation. The regular square network of indents with the step of 0.5 mm was performed in one quarter of each specimen after HPT. In order to find the exact centre of the specimen, two additional lines of indents on the other half of the specimen were also done. Using this procedure, the centre of each specimen was found with the accuracy of ±0.25 mm.

FEM simulations

Isothermal FEM simulations of the HPT process were carried out using the commercial rigid-plastic finite element code, DEFORM-3D ver. 6.1 [22]. A user-defined material subroutine for the three-dimensional (3D) version of the dislocation density-based constitutive model was employed [23, 24]. The number of initial meshes for the workpiece was 150,000, which was sufficient to show the local deformation behaviour.

Results and discussion

Dislocation density measurements

Figure 2 shows radial dependence of the mean positron lifetime for alloys subjected to various number of HPT revolutions. The mean lifetime is a robust parameter unaffected by mutual correlations between individual fitting parameters and can show general trends in studied samples. From inspection of Fig. 2, it becomes clear that during the first HPT revolution (i.e. in samples subjected to $N = ¼$, ½ and 1 turn), the mean lifetime increases with increasing strain, while for samples subjected to more than 1, HPT revolution gradually saturates. For the sample which was only pressed between the anvils ($N = 0$), there is no statistically significant difference between the mean lifetime at the periphery and at the centre. On the other hand, for all samples subjected to HPT deformation ($N > 0$), the mean lifetime is higher at the periphery than in the centre.

More information can be obtained from decomposition of positron lifetime spectra into the individual components. Positron lifetime spectra of all HPT deformed samples can be well described by two exponential components with lifetimes τ_1 and τ_2. Since the lifetime τ_1 of the shorter components is lower than the bulk positron lifetime in Mg $\tau_B = 225$ ps [25], it can be undoubtedly attributed to free positrons not trapped at defects. The longer component represents a contribution of positrons trapped at defects. The lifetime of the longer component $\tau_2 \approx 260$ ps is typical for positrons trapped at dislocations in Mg [26].

The dependence of the positron lifetimes τ_1, τ_2 on the radial distance r from the centre of the sample disk is plotted in Fig. 3 for specimens subjected to various number of HPT revolutions. Obviously, the lifetime τ_2 remains approximately constant testifying that the nature of positron traps remains unchanged, i.e. in all samples studied, positrons are trapped at dislocations. The lifetime τ_1 of the free positron component varies because of changes in density of defects. The relative intensity I_2 of the dislocation component is shown in Fig. 4. In the sample which was only pressed but not subjected to torsion straining ($N = 0$), the intensity I_2 remains approximately constant

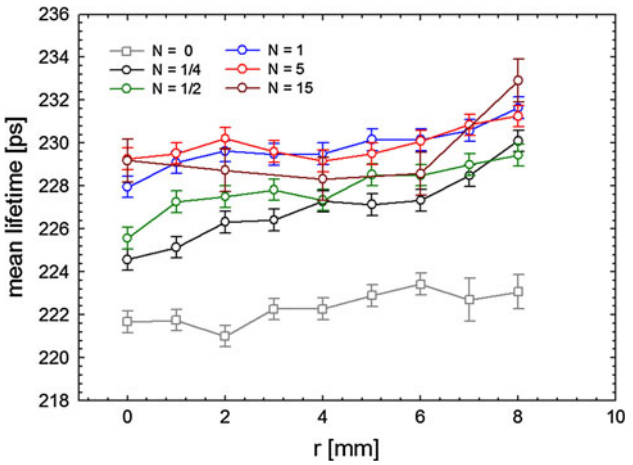

Fig. 2 Radial dependence of the mean positron lifetime for samples subjected to various number N of HPT revolutions

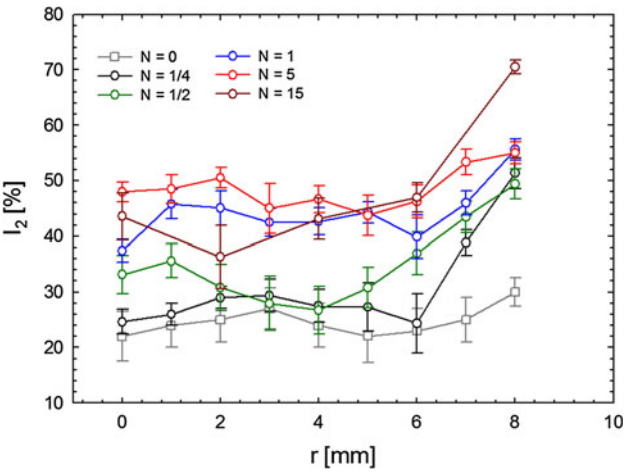

Fig. 4 Radial distance of the relative intensity I_2 of positrons trapped at dislocations for specimens subjected to various number N of HPT revolutions

across the sample. On the other hand, the samples subjected to HPT deformation ($N > 0$) exhibit enhanced intensity I_2 at the periphery. Hence, the dislocation density at the periphery is always higher than in the centre because of higher strain imposed at the periphery by HPT processing.

Dislocation density ρ_D can be calculated from positron lifetime data using the two-state simple trapping model [27]. The details of this procedure are described elsewhere [28].

Radial distances of the mean dislocation density ρ_D (calculated from Eq. (1) in [28]) for the samples subjected to various number of HPT revolutions are plotted in Fig. 5. From inspection of the figure, one can conclude that during HPT processing, the dislocation density increases firstly at the periphery (c.f. samples subjected to $N = ¼$ and ½ revolution) which is subjected to the highest strain. For samples subjected to more than half of HPT revolution, dislocation density increases also in the centre. However, the difference between the centre and the periphery (i.e. lower ρ_D in the centre and higher at the periphery) remains also in the samples subjected to more HPT revolutions. This can be clearly seen in Fig. 6 showing the dislocation density in the centre ($r = 0$ mm) and at the periphery ($r = 8$ mm) as a function on the number of HPT revolutions. The highest dislocation density was observed at the periphery of the sample subjected to 15 HPT revolutions. This sample exhibits also the largest difference between the dislocation density in the centre and at the periphery.

The dependence of the mean dislocation density ρ_D on the number of EX-ECAP passes is depicted in Fig. 7. The value ρ_D corresponding to 0 passes corresponds to the sample after extrusion only. The density of dislocation first increases during EX-ECAP processing and reaches its maximum in the sample subjected to 2 ECAP passes. However, further deformation leads to a decrease of dislocation density. This decline is caused by the process of

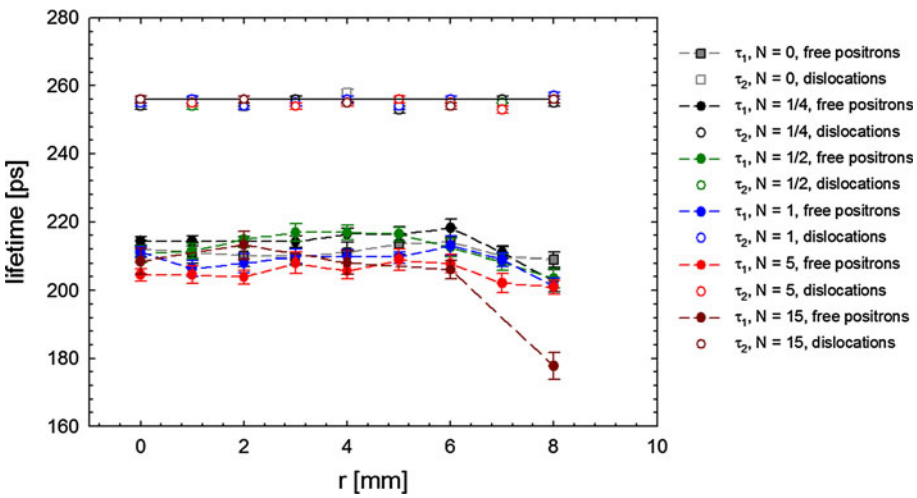

Fig. 3 Lifetimes τ_1, τ_2 of the components resolved in positron lifetime spectra as a function of the radial distance r from the centre of the sample for specimens subjected to various number N of HPT revolutions

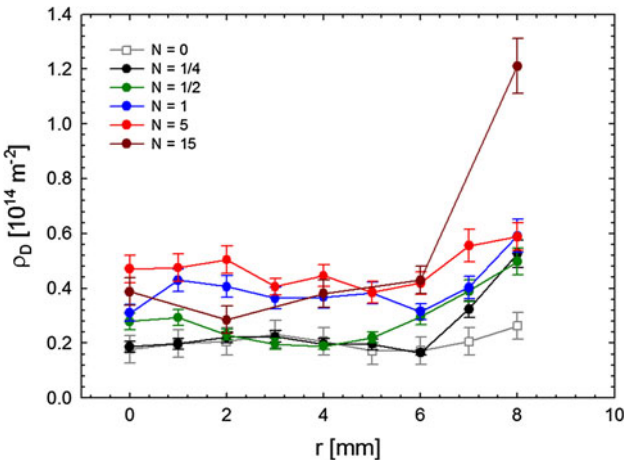

Fig. 5 Density of dislocations at various distances r from the centre of the sample disk for specimens subjected to various number N of HPT revolutions

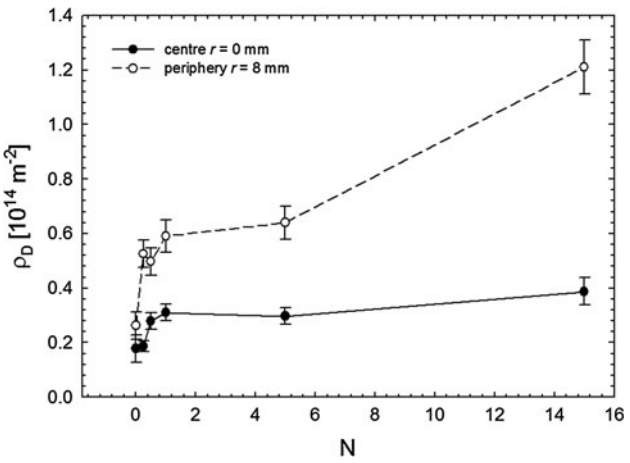

Fig. 6 Dependence of the dislocation density ρ_D in the centre ($r = 0$ mm) and at the periphery ($r = 8$ mm) for samples subjected to various number of HPT revolutions

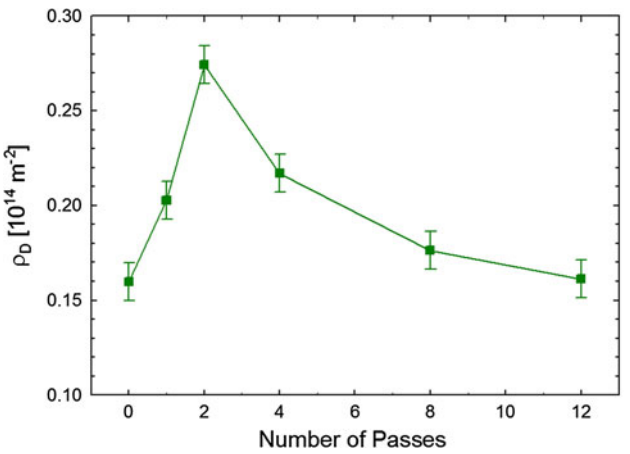

Fig. 7 The density of dislocations ρ_D of the specimens after extrusion and different number of ECAP passes [28]

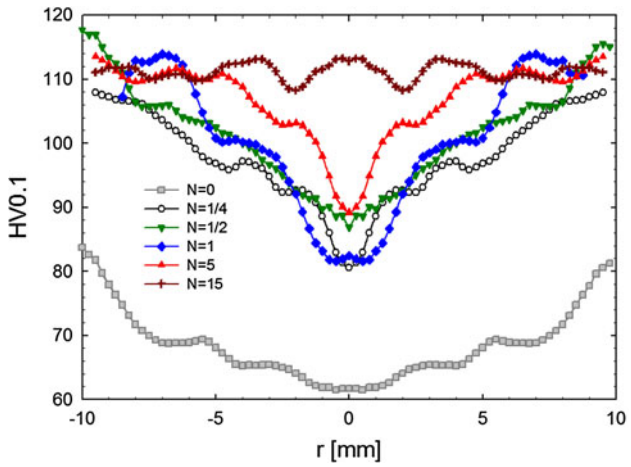

Fig. 8 Microhardness distribution across the diameter r of AZ31 disks after different number of rotations of HPT

recovery of dislocation structure during subsequent passes [28].

Microhardness measurements

Figure 8 shows the values of Vickers microhardness HV0.1 measured in linear traverses across the diameter of disks of AZ31 alloy after 0 (specimen was pressed only), ¼, ½, 1, 5 and 15 rotations of HPT at room temperature. Each data point was obtained as the average of four values obtained at the same distance from the centre of the disk. For clarity, the error bars are not shown in Fig. 8. The errors of the values are in the range of approximately 10 % (±5).

HPT straining introduces an inhomogeneity in the material which is manifested by a clear minimum in the microhardness values in the centre of the specimens after different number of rotations. Only the specimen after 15 rotations shows a relative homogeneity. The maximum microhardness measured in all specimens after rotation does not change a lot with increasing number of turns −HV values range from 108 to 115. The significant differences between microhardness values at the central and peripheral parts of the pressed-only sample (N = 0) could be explained by the different structures of high- and low-angle grain boundaries. Song et al. [29] studied grain boundary structure of the copper after compression stage of HTP by electron backscatter diffraction (EBSD) measurements and claimed that the amount of low-angle grain boundaries originating from dislocation activities increased significantly in the peripheral region of the samples. We observed slightly smaller grains in the peripheral part of the sample $N = 0$ in light microscope, but the higher amount of newly created low-angle grain boundaries could influence the microhardness values more.

The microhardness of samples after extrusion and ECAP is schematically shown in Fig. 9. The HV value

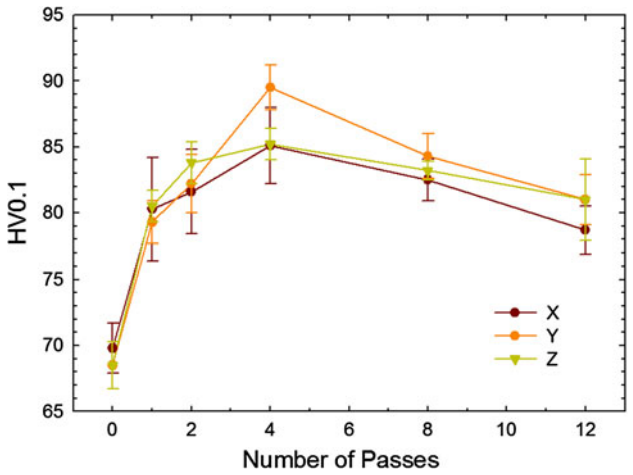

Fig. 9 Microhardness of the samples after extrusion and different number of ECAP passes

corresponding to 0 pass belongs to the sample after extrusion. The microhardness of the as-cast alloy is approximately equal to 58. We can see that the microhardness increases up to the fourth ECAP pass and then declines continuously with increasing strain. The HV values measured on all three reference planes (X, Y and Z) of the samples differ within the statistical error only. However, the textures of these individual samples differ not negligibly. Grains of extruded material have their crystallographic c-axis perpendicular to the extrusion direction (ED), i.e. <10.0> axes are parallel to the ED. On the contrary, texture of the extruded material after ECAP differs—the magnitude of rotation of the initial texture is equal to 40° [30].

Equivalent strain imposed by HPT and EX-ECAP

There are many ways by which we compare the mechanical properties, microstructure and defect density obtained by different techniques of SPD. Usually people compare the "effectiveness" of various techniques by comparing the respective properties at ultimate conditions, which in case of ECAP corresponds to the maximum number of passes while in HPT to the maximum number of turns. Such comparison reflects more of the experimental conditions used by each author rather than some physical reason.

As the evolution of microstructure and mechanical properties is controlled by equivalent strain imposed to the material during SPD, one of possible ways of making a more "objective" comparison is to take conditions of the same equivalent strain obtained by different techniques of SPD and to compare the respective microstructure, defect structure and mechanical properties of specimens processed by these techniques. In our case, we will compare the conditions of the same equivalent strain obtained by EX-ECAP and by HPT.

The effective strain (obtained from the FEM results) imposed by HPT increase at the centre after half a turn, while the torsion (shear) strain given by Eq. (1) is zero. The strain obtained by the FEM simulations at the centre, which is higher than the theoretical value [Eq. (1)], can be explained by the compressive strain in HPT and the finite mesh size in the FEM [19, 31]. The FEM simulation and torsion theory results are in a good agreement in the regions near the middle of the disk ($r = 4$–6 mm) after a single turn. However, at the periphery region ($r = 8$–10 mm), the results of the FEM simulations deviate from the theoretical values because of 'dead metal zone' phenomenon [31]. Therefore, the strain of middle region of the disk after HPT is well fitted according to the theoretical equation

$$\varepsilon = \frac{\gamma}{\sqrt{3}} = \frac{r\theta}{\sqrt{3}h}, \tag{1}$$

where γ is the shear strain, r is the radial distance from the centre of the disk-shaped workpiece, θ is the rotation angle, and h is the thickness of the workpiece.

The equivalent strain imposed by EX-ECAP could be calculated from the Eq. (1) in Chen et al. [32] and Eq. (6) in Valiev et al. [3]

$$\varepsilon_N = \ln R_E + \frac{2N}{\sqrt{3}}\cot\phi, \tag{2}$$

where, R_E is the extrusion ratio (equal to 22 in our case) and $\phi = \frac{\Phi}{2} = 45°$.

The plots of equivalent strains imposed by EX-ECAP and HPT are displayed in Fig. 10. Intersections of vertical lines (EX-ECAP) with "HPT" curves correspond to zones of the same equivalent strain in specimens processed by EX-ECAP and HPT which in HPT specimens are characterized by the distance r from the centre of the disk. The respective distances r corresponding to the intersections of the HPT and EX-ECAP curves from Fig. 10b are shown in Table 1. It is observed that owing to the inhomogeneous distribution of strain in specimens processed by HPT, one can find in each HPT specimen several zones corresponding to the same equivalent strain in several ECAP specimens (the rows of the table). On the other hand, to the strain imposed by ECAP in individual specimens' several zones of the same equivalent strain can be found in HPT specimens (the columns of the table).

Let us now compare the microhardness, dislocation density and microstructure in equivalent zones of ECAP and HPT specimens.

Microhardness values obtained in equivalent stain zones from the Table 1 are summarized in Table 2. Microhardness values measured in HPT samples are significantly

higher than the HV values in EX-ECAP samples (given in the first row of Table 2). This fact is probably caused by the different microstructure and dislocation density of the samples after HPT and EX-ECAP.

Microstructure of the extruded and 1P ECAP specimens is bimodal consisting of large (>10 μm) and small (~1 μm) grains. Microstructures of the specimens become more homogeneous and finer with increasing number of ECAP passes. Average grain sizes of the 4P, 8P, and 12P EX-ECAP specimens are approximately equal to 1 μm [30]. Microstructure of the samples after HPT was not yet investigated by EBSD which would give us detail information about microstructure in a relatively large scale. However, the local observations by transmission electron microscopy indicate that the initial coarse-grained microstructure transforms into inhomogeneous grain structure which becomes finer and more homogeneous with increasing number of HPT turns. The average grain sizes are reduced to ~ 100 nm in our case. These results are in good agreement with the similar observations of hexagonal Zr alloy after room temperature HPT done by Wang et al. [33]. They found an interesting structural evolution that is believed to be unique to hexagonal close packed materials and produces a structure with an inhomogeneous grain size distribution that later transforms into a uniform nanocrystalline structure with further HPT. Wang et al. claim that the inhomogeneous grain structure is clearly a transitional structure during grain refinement. With further deformation, grain rotations occurred and the internal inter-grain stresses built up, both of which favour the activation of dislocation slip systems [33].

The density of dislocations is the second principal factor influencing the microhardness values. Dislocation densities ρ_D shown in Tab. 3 were measured approximately in the same areas as the microhardness. Comparison of the values of dislocation densities is interesting. Dislocation densities measured at the peripheral parts of all samples after HPT and in the whole areas of the samples after 1, 5 and 15 turns

Table 1 Zones (characterized by the distance *r*) of the specimens after HPT corresponding to the same equivalent strain imposed by EX-ECAP

r [mm]	EX	1P	2P	4P	8P	12P
¼ N HPT	3–4	5	7	9		
½ N HPT	Centre	2	3	5	8	
1 N HPT				1	3–4	5–6

Table 2 Microhardness HV0.1 of the specimens after EX-ECAP and zones of the samples after HPT with the same equivalent strain

HV 0.1	EX	1P	2P	4P	8P	12P
	70	80	82	85	82	79
¼ N HPT	95–97	97	104	108		
½ N HPT	87	93	97	103	107	
1 N HPT				85	100	102–109

of HPT are significantly higher that ρ_D in specimens after EX-ECAP (given in the first row of Table 3). Higher values of dislocation densities in HPT specimens are probably caused by several reasons.

The first factor is the different processing temperature during HPT and EX-ECAP. It is well known that processing by ECAP had to be performed at elevated temperatures (180 °C in our case) as the hexagonal structure does not offer at normal conditions five independent slip systems which are required for uniform deformation according to von-Mises criterion [34]. On the other hand, other slip systems are operational not only at elevated temperatures but also at high stresses [35]. HPT was applied at room temperature because the hydrostatic pressure was high enough (2.5 GPa) to enable uniform deformation.

The other reason of higher dislocation densities in zones with the same equivalent strain in HPT specimens is the fact, that high applied pressure increases the stresses which can impede the cross-slip of screw dislocations depending

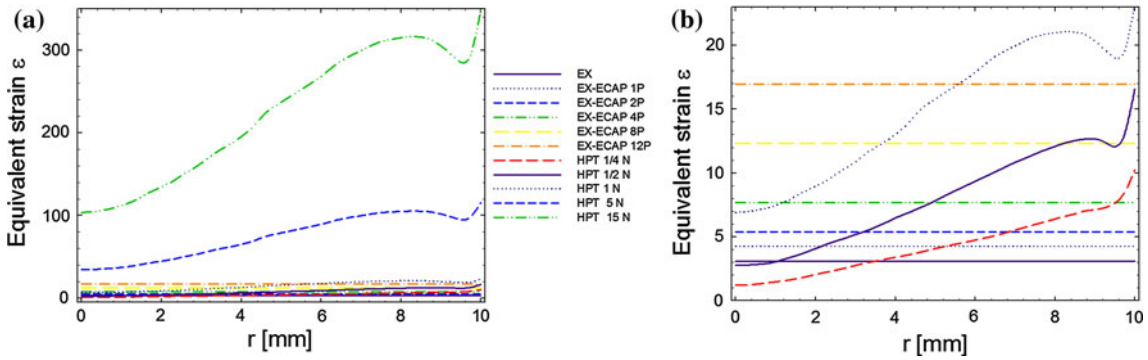

Fig. 10 Equivalent strains imposed by HPT and EX-ECAP (calculated from Eq. (1) and (2), respectively) shown in the full scale (**a**) and for small strains to highlight details (**b**)

Table 3 Dislocation density ρ_D of the specimens after EX-ECAP and zones of the samples after HPT with the same equivalent strain

ρ [10^{13} m^{-2}]	EX	1P	2P	4P	8P	12P
	1.6	2.0	2.7	2.2	1.8	1.6
¼ N HPT	2.1	2.0	3.2	–		
½ N HPT	2.8	2.3	2.0	2.2	5.0	
1 N HPT				4.3	3.6	3.5

on their orientation relative to the line and Burgers vectors [36]. AZ31 alloy has a low stacking fault energy (SFE) due to the pinning effect of alloying elements on grain boundaries and dislocations (SFE of pure magnesium is equal to 78 mJ m^{-2} [37], SFE of the AZ31 magnesium alloy is much smaller). The degree of dissociation of dislocations is therefore high which results in hindering of recovery by cross-slip and climb. However, the hindering stresses can further increase the degree of dislocation dissociation resulting in a difficult cross-slip and therefore in the obstruction of dislocation annihilation during HPT which also contributes to the high dislocation density [38].

Summary

Evolutions of mechanical properties, grain fragmentation and dislocation density in AZ31 magnesium alloy after two different SPD techniques (EX-ECAP and HPT) were investigated in this study. The equivalent strains imposed by EX-ECAP and HPT were calculated, and the variations in mechanical properties and dislocation density evolution were compared in conditions corresponding to the same equivalent strain imposed by both techniques of SPD. HPT proved to be more effective method of grain refinement of AZ31 alloy resulting in significantly higher values of microhardness and dislocation densities.

Acknowledgements This study was financially supported by the Czech Grant Agency (GACR) under the Grant 106/09/0482. J. Vrátná acknowledges the finacial support extended by GAUK 530712/2012 and SVV 2012-265303. J. Čížek acknowledges the support from GACR under the grant P108/10/064 and H.S. Kim acknowledges the financial support from POSCO by the project of mechanical joining for Mg alloys.

References

1. Gupta M, Sharon NML (2011) Magnesium, magnesium alloys, and magnesium composites. Wiley, Hoboken, p 1
2. Koch CC (2009) In: Zehetbauer MJ, Zhu YT (ed) Bulk nanostructured materials, Wiley, Weinheim, p 9
3. Valiev RZ, Langdon TG (2006) Prog Mater Sci 51:881
4. Zhilyaev AP, Langdon TG (2008) Prog Mater Sci 53:893
5. Kim HS (2001) J Mater Proc Tech 113:617
6. Saito Y, Utsunomiya H, Tsuji N, Sakai T (1999) Acta Mater 47:579
7. Varyutkhin VN, Beygelzimer Y, Synkov S, Orlov D (2006) Mater Sci Forum 503–504:335
8. Yang X, Okabe Y, Miura H, Sakai T (2012) J Mat Sci 47:2823. doi:10.1007/s10853-011-6111-6
9. Horita Z, Smith DJ, Furukawa M, Nemoto M, Valiev RZ, Langdon TG (1996) J Mater Res 11:1880
10. Yoon EY, Lee DJ, Kim T-S, Chae HJ, Jenei P, Gubicza J, Ungár T, Janeček M, Vrátná J, Lee S, Kim HS (2012) J Mat Sci 47:7117. doi:10.1007/s10853-012-6408-0
11. Zhilyaev AP, Nurislamova GV, Kim B-K, Baro MD, Szpunar JA, Langdon TG (2003) Acta Mater 51:753
12. Zhilyaev AP, Oh-ishi K, Langdon TG, McNelley TR (2005) Mater Sci Eng A410–411:277
13. Vrátná J, Janeček M, Stráský J, Kim HS, Yoon E-Y (2011) In: Sillekens WH, Agnew SR, Neelameggham NR, Mathaudhu SN (ed) Magnesium technology 2011, Wiley, New York, p 589
14. Harai Y, Ito Y, Horita Z (2008) Scripta Mater 58:469
15. Zhilyaev AP, Langdon TG (2012) J Mat Sci 47:7888. doi:10.1007/s10853-012-6429-8
16. Bonarski BJ, Schafler E, Mingler B, Skrotzki W, Mikulowski B, Zehetbauer MJ (2008) J Mat Sci 43:7513. doi:10.1007/s10853-008-2794-8
17. Joo SH, Yoon SC, Lee CS, Nam DH, Hong SH, Kim HS (2010) J Mat Sci 45:4652. doi:10.1007/s10853-010-4382-y
18. Jenei P, Yoon EY, Gubicza J, Kim HS, Lábár J, Ungár T (2011) Mater Sci Eng A 528:4690
19. Song Y, Yoon EY, Lee DJ, Lee JH, Kim HS (2011) Mat Sci Eng A 528:4840
20. Bečvář F, Čížek J, Lešták L, Novotný I, Procházka I, Šebesta F (2000) Nucl Instrum Method A 443:557
21. Procházka I, Novotný I, Bečvář F (1997) Mater Sci Forum 255–257:772
22. DEFORM software, Scientific Forming Technologies Corp., Columbus, OH (2007)
23. Tóth LS, Molinari A, Estrin Y (2002) J Eng Mater Technol 124:71
24. Baik SC, Estrin Y, Kim HS, Hellmig RJ (2003) Mater Sci Eng A 351:86
25. Čížek J, Procházka I, Smola B, Stulíková I, Kužel R, Matěj Z, Cherkaska V (2006) Phys Stat Sol (A) 203:466
26. Čížek J, Procházka I, Smola B, Stulíková I, Očenášek V (2007) J Alloys Comp 430:92
27. West R (1979) In: Hautojärvi P (ed) Positrons in Solids Springer, Berlin, p 89
28. Janeček M, Čížek J, Gubicza J, Vrátná J (2012) J Mat Sci 47:7860. doi:10.1007/s10853-012-6538-4
29. Song Y, Yoon EY, Lee DJ, Lee JH, Kim HS (2011) Mater Sci Eng A 528:4840
30. Janeček M, Yi S, Král R, Vrátná J, Kainer KU (2010) J Mater Sci 45:4665. doi:10.1007/s10853-010-4675-1
31. Lee DJ, Yoon EY, Park LJ, Kim HS (2012) Scripta Mater 67:384
32. Chen Y, Wang Q, Peng J, Zhai C, Ding W (2007) J Mat Proc Tech 182:281
33. Wang YB, Louie M, Cao Y, Liao XZ, Li HJ, Ringer SP, Zhu YT (2010) Scripta Mater 62:214
34. Von Mises R (1928) Angew Z Math Mech 8:161
35. Hirth JP, Lothe J (1982) Theory of Dislocations, 2nd edn. Wiley, New York, p 277
36. Gubicza J, Chinh NQ, Lábár JL, Hegedűs Z, Langdon TG (2010) Mater Sci Eng A 527:752
37. Sastry DH, Prasad YVRK, Vasu KI (1969) Scripta Mater 3:923
38. Gubicza J, Chinh NQ, Dobatkin SV, Khosravi E, Langdon TG (2011) Key Eng Mater 465:195